ADVANCED MATERIALS
www.advmat.de

Reprogrammable Phononic Metasurfaces

Osama R. Bilal, André Foehr, and Chiara Daraio**

Phononic metamaterials rely on the presence of resonances in a structured medium to control the propagation of elastic waves. Their response depends on the geometry of their fundamental building blocks. A major challenge in metamaterials design is the realization of basic building blocks that can be tuned dynamically. Here, a metamaterial plate is realized that can be dynamically tuned by harnessing geometric and magnetic nonlinearities in the individual unit cells. The proposed tuning mechanism allows a stiffness variability of the individual unit cells and can control the amplitude of transmitted excitation through the plate over three orders of magnitude. The concepts can be extended to metamaterials at different scales, and they can be applied in a broad range of engineering applications, from seismic shielding at low frequency to ultrasonic cloaking at higher frequency ranges.

Phonons are lattice vibrations that are responsible for the propagation of sound, vibrations (at low frequencies) and heat (at higher frequencies). Our ability to understand and control phonons in these different domains are of extreme importance for practical applications and engineering devices, such as acoustic lenses and cloaking materials.[1–4] Phononic crystals and metamaterials are material systems that exploit the geometry and elastic properties of basic building blocks (the unit cells), often repeating in space, to manipulate phonons and redirect energy. Elastic metamaterials can present peculiar properties, such as negative effective density and stiffness.[5–7] Phononic materials can be designed to present bandgaps, which are frequency ranges where waves can't propagate. When the metamaterials present resonances in their fundamental unit cells, the bandgaps can occur at subwavelength frequencies, reflecting waves with wavelengths much larger than the size of the unit cells.[8]

The linear response of phononic crystals and metamaterials has been studied extensively.[1] However, the number of studies concerning nonlinear phononic materials is quite scarce in comparison to linear analyses.[3,9] The richness of the dynamic responses arising in nonlinear metamaterials is substantial, including phenomena with no linear parallel, such as bifurcations, chaos, and solitary waves formation.[10–13] Metamaterials, both linear and nonlinear, can be used for filtering,[14] localization,[15] focusing,[16,17] lensing,[18] cloaking,[19] and guiding of waves.[20,21] Potential applications of phononic metamaterials vary across a broad range of scales, from seismic wave protection[22] to heat shielding.[23]

Owing to their physical realization, locally resonant metamaterials retain narrow subwavelength bandgaps. Moreover, the fixed geometry and dimensions of the unit cell set a hardbound on the central frequency of the operational bandwidth. There exist many demonstrations of tunable phononic crystals (such as in references[24,25] and the references within), some of which utilize an external magnetic field.[26–28] Other methods to tune phononic metamaterials include piezo shunting,[29] cell symmetry relaxation,[30] embedded electromagnets,[31] static loading,[32] granular contacts,[33,34] and acoustic trapping.[35] However, these metamaterials either lack the locality of element-wise programming, they continuously consume energy, or lack the ability to switch dynamically between desired material functionalities. Moreover, most existing tunable metamaterials require direct contact between the metamaterial and the programming method. Obtaining element-wise and real-time programmability of metamaterials, in a reversible manner, would allow their applications in new sensors, filters, and switches. Here, we realize a metamaterial plate that uses nonlinear interactions between its unit cells and an external magnetic potential. This allows dynamic tuning of the wave propagation, within 300 ms, controlling the frequency range of deep subwavelength bandgaps. We refer to our metamaterial as reprogrammable, because it can be dynamically tuned spatio-temporally and the tuning is reversible.

The realized metamaterial plate is composed of spiral-spring unit cells,[36] periodically repeated in the x- and y-directions to form a 28×20 array (**Figure 1**a,b). Each unit cell is composed of four concentric Archimedean spirals with a magnet embedded in its center. The resonators have a quality factor, Q, of ≈52 (see Supporting Information). This design has the ability to attenuate a range of ultralow frequencies in all directions, supporting the formation of a complete bandgap between 89 and 126 Hz (gray shaded region in Figure 1c). The out-of-plane unit cell mode shape, at the edge of the attenuated range is responsible for forming the bandgap. Varying the stiffness of this

Dr. O. R. Bilal
Institute for Theoretical Physics
ETH Zurich
Zurich 8092, Switzerland
E-mail: bilalo@ethz.ch

Dr. O. R. Bilal, A. Foehr
Department of Mechanical and Process Engineering
ETH Zurich
Zurich 8092, Switzerland

Dr. O. R. Bilal, A. Foehr, Prof. C. Daraio
Division of Engineering and Applied Science
California Institute of Technology
Pasadena, CA 91125, USA
E-mail: daraio@caltech.edu

The ORCID identification number(s) for the author(s) of this article can be found under https://doi.org/10.1002/adma.201700628.

DOI: 10.1002/adma.201700628

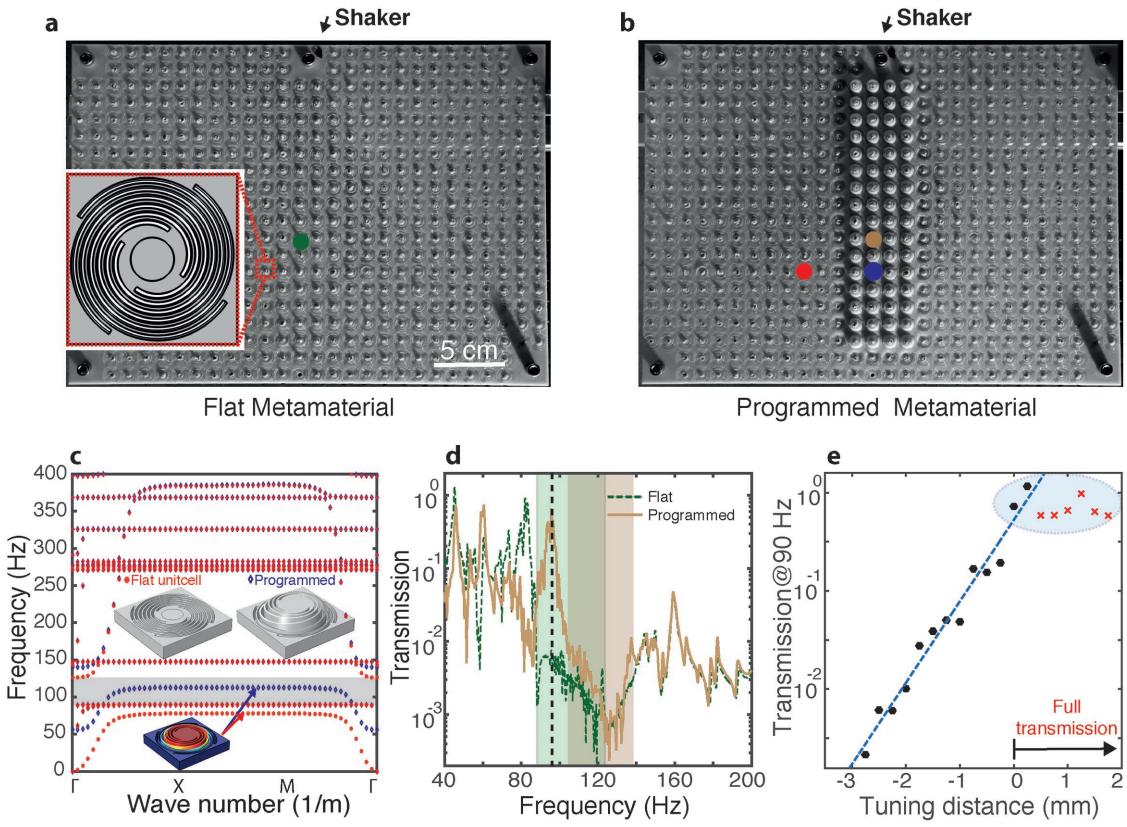

Figure 1. Metamaterial programming concept: a,b) Fabricated metamaterial with 28 × 20 cells in the flat 2D configuration (a) and in the programmed 3D state (b). c) Numerically predicted dispersion curves for both configurations. The gray shaded region corresponds to the bandgap for the flat unit cell. The magnetic forces at the center of the unit cells have been incorporated in the model as spring foundations. d) Frequency response functions of the two configurations with the bandgap for the "flat" configuration shown by the green shaded region. The bandgap for the "programmed" configuration is shown in brown shading. The dashed line indicates the frequency $f = 96$ Hz. e) The transmission at a single frequency, $f = 90$ Hz, as a function of tuning distance of the magnets from the metamaterial plate. The blue shaded area represents the maximum transmission region.

particular mode, it is possible to tune the edge of the bandgap to higher or lower frequencies. We use noncontact magnetic forces to vary the stiffness of the unit cells (by displacing the spring in and out of plane) and tune the metamaterial's dispersion relation. Underneath the metamaterial plate, we place an array of permanent magnets (referred to as the "tuning magnets"), used to create a controllable magnetic potential that can be tuned by moving the magnets closer to or further away from the metamaterial plate (along the z-axis). As the magnets approach the unit cells, repulsion forces intensify nonlinearly (Figure S1, Supporting Information). When the tuning magnets are close to the metamaterial plate, the unit cells transform from a 2D, "flat" configuration into a 3D, "programmed" geometry, Figure 1a,b. This shape change alters the effective stiffness of the resonators and the calculated dispersion relation (see Figure S2, Supporting Information) of the plate (Figure 1c). We confirmed this experimentally, measuring the transmission spectrum of harmonic elastic vibrations propagating through the plate (Figure 1d), (see the Experimental Section and Supporting Information). The gray shaded region in Figure 1d is the predicted bandgap range corresponding to Figure 1c. When the tuning magnets are close to the plate ("programmed" configuration) the bandgap edge shifts to around 96 Hz within the bandgap area of the "flat" configuration. This shows a binary (digital) programmability of the material, at a given frequency, from transmission to no-transmission states and vice versa. However, by controlling the strength of the magnetic field (i.e., the position of the magnetic tuning stage), the material's programmability can be used either as a binary (On/Off transmission) or analog. In order to show the analog (continuous) programmability of the phononic properties of the material, we plot the measured transmission amplitude as a function of the distance between the tuning magnets and the plate, in Figure 1e. The zero point is defined as the first full transmission value, after which the system is in a pass band. Before full transmission, the material shows continuous tuning behavior, from complete attenuation to full transmission in a linear fashion (the fitted dashed blue line considers only the black dots before full transmission). This corresponds to a transmission tunability that spans approximately three orders of magnitude.

In order to investigate the tunability of the metamaterial in time, we first model the transformation of a single unit cell from the flat (2D) to programmed (3D) configuration and vice

versa. We use finite element analysis to determine the effective stiffness of the unit cell for the different measured magnetic forces from Figure S1 (Supporting Information). Then, we formulate the equation of motion of the system using the stiffness of the unit cell and the tuning time to calculate the initial oscillations of the resonator center around its equilibrium position (overshoot). In our current configuration, chosen as a proof of principle, the linear stage controlling the array of magnets can tune the geometry of the unit cells in ≈300 ms. This tuning speed leads to a maximum overshoot of the center of the resonator from its final position of about 0.5% (**Figure 2**a). It is worth noting that the center of the unit cell oscillates around ≈89 Hz when transforming from 3D to 2D and around ≈105 Hz from 2D to 3D. These two frequencies correlate to the lower edge of the bandgap in the flat and the programmed configurations. The increase in the resonance frequency from 89 to 105 Hz is due to the added stiffness to the mode shape at the edge of the bandgap. This tuning speed can be significantly increased, using either a faster stage or electromagnets in place of the permanent magnets. We use the same model to calculate the deflection overshoot as a function of tuning time in a log–log plot in Figure 2b. This suggests an overshoot of as low as 1% for a tuning time of 10 ms.

In order to demonstrate the ability to change the metamaterial's phononic properties in time, we program the magnetic array underneath the metaplate (fixed to a linear stage) to move up and down in different time windows (Figure 2c-top). We continuously excite the system harmonically at 96 Hz and measure the transmission through the material at the blue and red dots in Figure 1b. The measured transmitted wave inside the tuned spirals (blue line in Figure 1c-center) follows the programmed temporal pattern (black line in Figure 1c-top), showing a clear distinction between transmission and no-transmission states. The measured transmitted wave signal at the red dot (outside the controlled region) is immune to the changes taking place in the rest of the system (red line in Figure 1c-bottom), despite the fact that the red dot is only three unit cells away from the transmission guide. This implies robustness of the system and shows the locality of the element-wise control of the unit cells in the metamaterial. The fast Fourier transform (FFT) of the transmission signal inside the controlled region (Figure 1c-center) for the time windows in both configurations

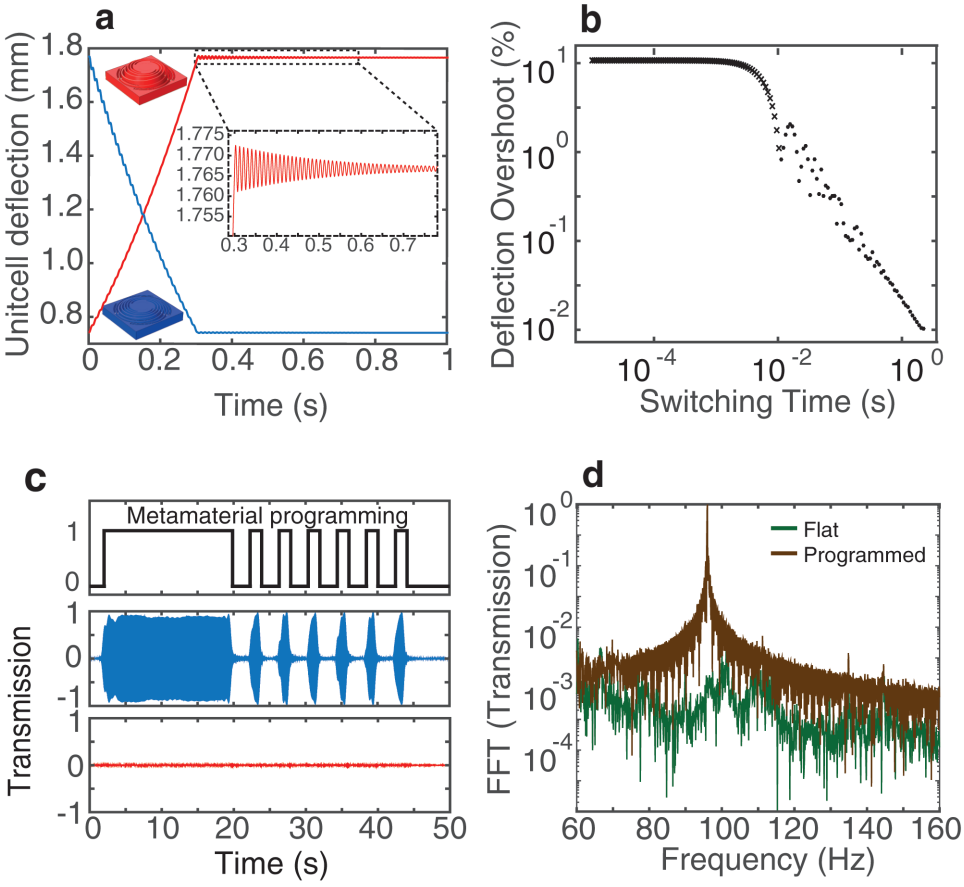

Figure 2. Metamaterial temporal programming: a) Numerical analysis of the interaction between the magnetic field and a single unit cell deflection of 1 mm when transformed from 2D to 3D (and vice versa) within 300 ms time interval and the transient deflection overshoot in the zoomed in inset. b) The deflection overshoot error percentage plotted as a function of switching speeds ranging from 10 µs to 2 s. c) Preprogrammed temporal pattern of the metamaterial in time (top), transmitted signal at the blue dot in Figure 1b within the programmed region (center), and the transmitted signal at the red dot in Figure 1b outside the programmed guide. The utilized stage can move between the two programming positions (i.e., On/Off) in ≈300 ms. d) FFT of the transmitted signal when the unit cell is 3D "programmed" and 2D "flat."

flat and programmed is plotted in Figure 2d. The FFT for the "programmed" state shows the single frequency content of the transmitted signal, while the "flat" state FFT demonstrates the absence of any significant frequency content. Moreover, the behavior of the system doesn't deteriorate over time after repeating the switching cycles ≈1000 times, indicating the absence of plastic deformation or damage in the material.

To investigate the wave propagation characteristics throughout the entire plate, we first select two different frequencies; one within the pass band (f_1 = 84 Hz) and the other in the stop band frequency (f_2 = 96 Hz). We excite the plate with out-of-plane, harmonic vibrations on its top side, using a mechanical shaker (see the Experimental Section) with f_1 and f_2 separately. We scan the plate using a laser vibrometer to record the wave velocity at the center of each unit cell. Then we plot the transmission data for each of the frequencies as a heat map (**Figure 3**a,b). Within the pass band frequency (f_1 = 84 Hz), Figure 2a, full propagation of the wave throughout the plate exists. In the stop band frequency f_2, we record an exponential decay in transmission amplitude (Figure 2b). In both cases, there is an intense radial wave field close to the source (top center of the plate), because of the inherent damping of the material (Figure S3, Supporting Information). We note that the displacement of the plate due to its resonant modes cannot be resolved in the measured signals, as it correlates to much lower frequencies.

To explore the limits of the element-wise control and exploit the versatility of the presented platform, we control the spatial energy propagation designing more "complex" waveguides on the metamaterial plate. Because of the ability to tune individual elements, it is possible to create a vast number of wave guiding configurations. If a higher resolution wave-guiding ability is needed, it is possible to add more unit cells in both directions. We choose to present one of these configurations, which resemble an ETH logo (Figure 3c,d; Movie S1, Supporting Information). Similar to the former wave propagation scans in Figure 3a,b, we excite the plate harmonically from the middle of its top side, and scan the transmission pattern throughout the plate. The intensity of the transmitted waves (Figure 3d) clearly highlights the logo's profile. It should be noted that the letters E, T, and H are close to the vibration source and they expand the radial decaying pattern observed in Figure 3a,b to span the entire plate width. It is evident that the metamaterial requires 3–4 unit cells to significantly attenuate the waves.[37,38] This decay distance should be accounted for in the design of potential applications. The ability to tune the individual cells continuously (analog tuning) presented in Figure 1e, allows the realization of metamaterial plates with an infinite number of possible wave propagation pathways.

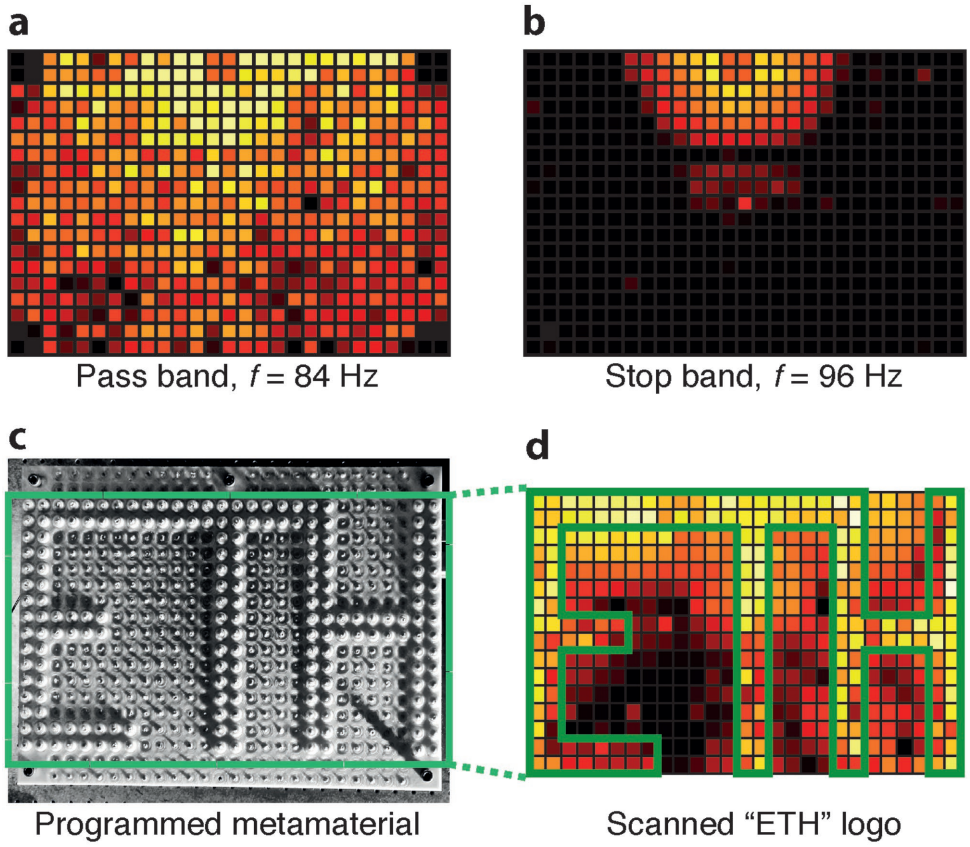

Figure 3. Metamaterial spatial programming: a,b) Particle velocity scans of the metamaterial when excited at the top-center harmonically within a pass band (a) and a stop band (b). c,d) The ETH logo programmed using magnetic potentials (c) and its corresponding scan when excited harmonically at 96 Hz (d).

The experiments discussed show the ability to tune the dynamic response of the plate either in time (Figure 2) or in space (Figure 3). In many practical applications, however, it is desirable to be able to reconfigure dynamically the spatial propagation of waves in a medium, for example, to selectively mitigate vibrations in precise areas of a surface, which could vary with time. Our proposed metamaterial plate achieves this functionality by varying the position of the tuning magnets in space and time, simultaneously.

We demonstrate this experimentally in a waveguide with a 90 degrees bending angle, which redirects excitations from the top side of the plate to a different position along the right edge (marked with an "x" in **Figure 4**a). We create this waveguide using magnets mounted on a movable rail. To visualize the dynamics of the plate, we use a laser scanning vibrometer and plot the vibration amplitude transmitted through the plate in Figure 4b. The time signal of the propagating wave at time = 0 s is presented in Figure 4c. We then program the horizontal stage to move toward the lower edge of the waveguide, Figure 4d. When the stage stops (at time = 18 s), we scan the plate once more to observe the change in wave transmission through the waveguide (Figure 4e). Similar to the data presented in Figure 4c, we record the time signal at the green X mark in Figure 4f. Both panels c and f in Figure 4 show the immunity of the transmitted signal to noise, when the waveguide is evolving from one state to the other. The time spanned between the two states (from the blue X to the green X) can be reduced significantly by using faster stages or by utilizing

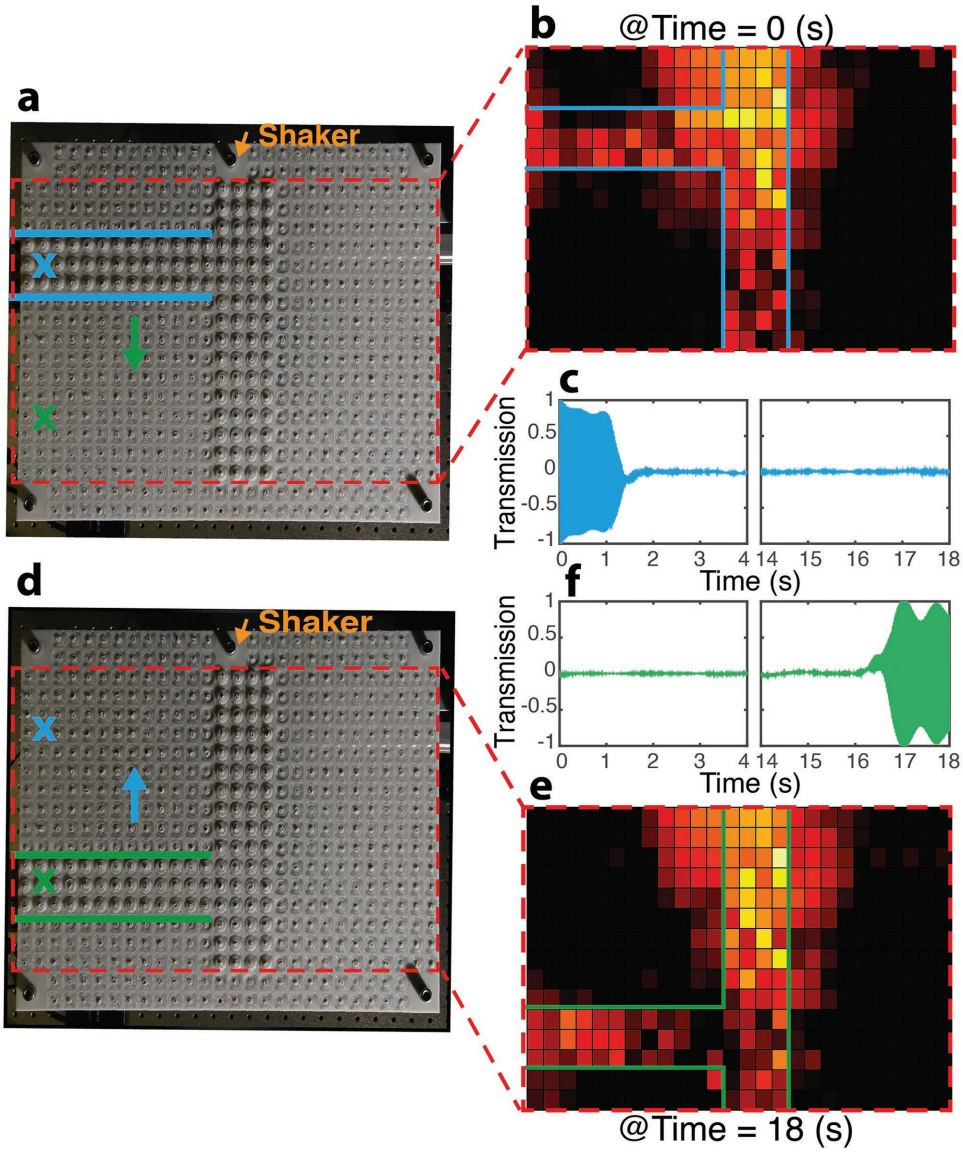

Figure 4. Metamaterial spatio-temporal programming: a) Vertical wave-guiding channel, with a bend toward the top left corner (blue X marker) of the plate. b) Experimental scan of transmitted waves throughout the spatially programmed pattern in (a). c) The measured transmission signal at the blue X marker in time. d) The reprogrammed metamaterial, now with a bend toward the green X marker. f) Measured time signal at the green X marker during the reprogramming process. e) Experimental scan of the transmitted signal through the metamaterial after the reprogramming.

electromagnetic tuning elements for controlling the individual resonators.

This work presents the design and the experimental realization of a tunable phononic metamaterial with programmable deep subwavelength bandgaps. We dynamically control the wave propagation through the metamaterial, switching the signal in time and guiding it in space, using a noninvasive element-wise magnetic potential. This reversible "programmability" of the metamaterial, resolved at the unit cell level, can have impact in the design of advanced functional materials, programmable matter and transducers for acoustic imaging, lensing, and nondestructive evaluation devices.

Experimental Section

For the fabrication of the metamaterial this study utilized a Fortus 400 3D printer by Stratasys. The lattice spacing between the metamaterial unit cells was 12.5 mm. Cylindrical neodymium-nickel-plated magnets, with a 3 mm diameter and a 2 mm thickness, were embedded in the center of each unit cell. The utilized printing material was polycarbonate with Young's modulus of 2.3 GPa and density of 1200 Kg m^{-3}, as provided by the supplier. The measured quality factor of the metamaterial was ≈52 (Figure S3, Supporting Information). A medium-density fiberboard (MDF) plate with 28 × 16 cylindrical holes was placed underneath the metamaterial plate. Each hole can fit a magnet strong enough to tune the phononic properties of the metamaterial (by transforming the unit cells from 2D to 3D). The array of control magnets with a 5 mm diameter and 4 mm thickness was placed on a movable stage, bislide of type PK206-03A-P1, below the array of unit cells, to tune the intensity of the magnetic field. For the space-time reprogrammability in Figure 4, two independent MDF plates (13 × 3 and 16 × 4 magnets) were mounted perpendicular to each other on a linear stage, with the ability to move in the x–y plane. Then the joint part (the two perpendicular stages) was mounted on a vertical linear stage to achieve the mobility in the z direction.

Mechanical oscillations in the metamaterial were excited using a Mini-shaker (Brüel & Kjær Type 4810) with an audio amplifier (Topping TP22), and were then optically detected by a laser Doppler vibrometer (Polytec OFV-505 with an OFV-5000 decoder, using a VD-06 decoder card). A drop of glue mixed with micro glass spheres was added to the center of each resonator (targeted by the laser Doppler vibrometer for measurements) to enhance the quality of the reflected signal. A lock-in amplifier from Zürich Instruments (HF2LI) was used to filter the signal. The transmission in Figure 1d,e was defined as the ratio between the measured velocity signals by the laser vibrometer at the point of interest over the one measured at the input (at the shaker location). The magnetic forces were characterized using a standard compression test with an Instron E3000. The dispersion curves were obtained using 3D finite element assuming Bloch boundary conditions in both x- and y-directions, while the z-direction had a free boundary (See Supporting Information). The numerical analysis in Figure 2a,b incorporates the experimentally measured magnetic forces (see the Supporting Information). The time series in Figure 2c, 4c,f were obtained using an oscilloscope (Tektronix DPO3014) and filtered using a pass-band filter at 96 Hz with a window width of 80 Hz. The FFT in Figure 2d was calculated on the raw (unfiltered) signal. All the numerical simulations were done in COMSOL 5.1 using the structural mechanics module.

Supporting Information

Supporting Information is available from the Wiley Online Library or from the authors.

Acknowledgements

The authors thank T. Jung for help with the additive manufacturing. This work was supported by the ETH Postdoctoral Fellowship FEL-26 15-2 to O.R. Bilal and ETH Grant No. ETH-24 15-2.

Conflict of Interest

The authors declare no conflict of interest.

Keywords

adaptive waveguiding, analog and digital materials, phononic metamaterials, programmable materials, real-time tunability

Received: February 3, 2017
Revised: May 15, 2017
Published online:

[1] A. Khelif, A. Adibi, *Phononic Crystals: Fundamentals and Applications*-Springer, **2015**.
[2] S. A. Cummer, J. Christensen, A. Alù, *Nat. Rev. Mater.* **2016**, *1*, 16001.
[3] M. I. Hussein, M. J. Leamy, M. Ruzzene, *Appl. Mech. Rev.* **2014**, *66*, 040802.
[4] M. Maldovan, *Nature* **2013**, *503*, 209.
[5] J. Li, C. Chan, *Phys. Rev. E* **2004**, *70*, 055602.
[6] N. Fang, D. Xi, J. Xu, M. Ambati, W. Srituravanich, C. Sun, X. Zhang, *Nat. Mater.* **2006**, *5*, 452.
[7] Y. Ding, Z. Liu, C. Qiu, J. Shi, *Phys. Rev. Lett.* **2007**, *99*, 093904.
[8] Z. Liu, X. Zhang, Y. Mao, Y. Zhu, Z. Yang, C. Chan, P. Sheng, *Science* **2000**, *289*, 1734.
[9] S. Mohammadi, A. Khelif, A. Adibi, in *Phononic Crystals*, (Ed. A. Khelif, A. Adibi), Springer, **2016**, pp. 239–245.
[10] G. Theocharis, N. Boechler, C. Daraio, in *Acoustic Metamaterials and Phononic Crystals*, Springer, **2013**, pp. 217–251.
[11] F. Romeo, M. Ruzzene, *Wave Propagation in Linear and Nonlinear Periodic Media: Analysis and Applications*, Vol. *540*, Springer Science & Business Media, **2013**.
[12] V. Nesterenko, *Dynamics of Heterogeneous Materials* Springer Science & Business Media, **2013**.
[13] S. H. Strogatz, *Nonlinear Dynamics and Chaos: with Applications to Physics, Biology, Chemistry, and Engineering*, Westview Press, **2014**.
[14] Y. Pennec, B. Djafari-Rouhani, J. Vasseur, A. Khelif, P. Deymier, *Phys. Rev. E* **2004**, *69*, 046608.
[15] N. Boechler, G. Theocharis, S. Job, P. Kevrekidis, M. A. Porter, C. Daraio, *Phys. Rev. Lett.* **2010**, *104*, 244302.
[16] A. Spadoni, C. Daraio, *Proc. Natl. Acad. Sci. USA* **2010**, *107*, 7230.
[17] S. Guenneau, A. Movchan, G. Pétursson, S. A. Ramakrishna, *New J. Phys.* **2007**, *9*, 399.
[18] M. Ambati, N. Fang, C. Sun, X. Zhang, *Phys. Rev. B* **2007**, *75*, 195447.
[19] D. Torrent, J. Sánchez-Dehesa, *New J. Phys.* **2008**, *10*, 063015.
[20] M. Torres, F. M. de Espinosa, D. Garcia-Pablos, N. Garcia, *Phys. Rev. Lett.* **1999**, *82*, 3054.
[21] O. R. Bilal, M. I. Hussein, *Appl. Phys. Lett.* **2013**, *103*, 111901.
[22] S.-H. Kim, M. P. Das, *Mod. Phys. Lett. B* **2012**, *26*, 1250105.
[23] S. Narayana, Y. Sato, *Phys. Rev. Lett.* **2012**, *108*, 214303.
[24] O. B. Matar, J. Vasseur, P. A. Deymier, in *Acoustic Metamaterials and Phononic Crystals* Springer, **2013**, pp. 253–280.
[25] A. Bergamini, T. Delpero, L. D. Simoni, L. D. Lillo, M. Ruzzene, P. Ermanni, *Adv. Mater.* **2014**, *26*, 1343.

[26] J.-F. Robillard, O. B. Matar, J. Vasseur, P. Deymier, M. Stippinger, A.-C. Hladky-Hennion, Y. Pennec, B. Djafari-Rouhani, *Appl. Phys. Lett.* **2009**, *95*, 124104.
[27] J. Vasseur, O. B. Matar, J. Robillard, A.-C. Hladky-Hennion, P. A. Deymier, *AIP Adv.* **2011**, *1*, 041904.
[28] F. Allein, V. Tournat, V. Gusev, G. Theocharis, *Appl. Phys. Lett.* **2016**, *108*, 161903.
[29] Z. Hou, B. M. Assouar, *Appl. Phys. Lett.* **2015**, *106*, 251901.
[30] P. Celli, S. Gonella, *Appl. Phys. Lett.* **2015**, *106*, 091905.
[31] Z. Wang, Q. Zhang, K. Zhang, G. Hu, *Adv. Mater.* **2016**, *28*, 9857.
[32] P. Wang, F. Casadei, S. Shan, J. C. Weaver, K. Bertoldi, *Phys. Rev. Lett.* **2014**, *113*, 014301.
[33] N. Boechler, G. Theocharis, C. Daraio, *Nat. Mater.* **2011**, *10*, 665.
[34] F. Li, P. Anzel, J. Yang, P. G. Kevrekidis, C. Daraio, *Nat. Commun.* **2014**, 5.
[35] M. Caleap, B. W. Drinkwater, *Proc. Natl. Acad. Sci. USA* **2014**, *111*, 6226.
[36] O. R. Bilal, A. Foehr, C. Daraio, *Proc. Natl. Acad. Sci. USA* **2017**, *114*, 4603.
[37] M. Rupin, F. Lemoult, G. Lerosey, P. Roux, *Phys. Rev. Lett.* **2014**, *112*, 234301.
[38] P. Celli, S. Gonella, *App. Phys. Lett.* **2015**, *107*, 081901.